Bull. Inst. Chem. Res., Kyoto Univ., Vol. 68, No. 2, 1990

Identification of New Isotopes with the He-Jet Fed On-Line Isotope Separator KUR-ISOL

Kotoyuki OKANO* and Yoichi KAWASE*

Received July 30, 1990

The He-jet fed isotope separator on-line (ISOL) facility, KUR-ISOL, has been constructed for the studies on nuclei far from stability produced by fission. The separator can give high-intensity beams of rare-earth elements using a high-temperature thermal ion source. Four neutron-rich isotopes in the rare-earth region, ^{152}Ce, ^{154}Pr, ^{155}Nd and ^{156}Pm have so far been newly identified at this facility. The methods of identification and the implications of the results are presented together with some technical developments on the KUR-ISOL facility recently performed.

KEY WORDS: ^{152}Ce, ^{154}Pr, ^{155}Nd, ^{156}Pm, new isotope, KUR-ISOL

INTRODUCTION

An isotope separator for the separation of stable isotopes has been constructed by Profs. K. Kimura, H. Takekoshi *et al.* in the Institute for Chemical Research, Kyoto University, in 1956[1]. The electronic systems of the separator such as current and voltage stabilizers have been designed and constructed by Prof. H. Takekoshi. The separated isotopes were used for the studies of nuclear reactions and nuclear structure until the separator was decided to be broken up in 1975. Then almost all the pieces of the separator were moved to the Keage Laboratory of the Institute for Chemical Research, although several pieces were moved to the Research Reactor Institute, Kyoto University, for the construction of a test separator for a new ISOL which was to be installed at a planned high-flux reactor. As the construction of the planned high-flux reactor was delayed, the test machine attached to the KUR (Kyoto University Reactor) was gradually graded up and now its perfomance exceeds that of similar apparatus in other countries in some respects. By using this separator (KUR-ISOL), the search for fission-produced very neutron-rich isotopes in the rare-earch region has been performed and four isotopes, ^{152}Ce, ^{154}Pr, ^{155}Nd and ^{156}Pm, have hitherto been newly identified. The methods and implications of the identification are described together with some developments on the KUR-ISOL facility recently performed.

EXPERIMENTAL APPARATUS

i) *Basic layout of KUR-ISOL*

A schematic diagram of the apparatus is shown in Fig. 1. The target material of 93% enriched ^{235}U is irradiated by the neutron flux of maximum 3×10^{12} n/cm^2 • s at the through-tube facility of the KUR. The recoiled fission products are slowed down

* 岡野事行, 川瀬洋一: Research Reactor Institute, Kyoto University, Kumatori-cho, Sennan-gun, Osaka 590-04

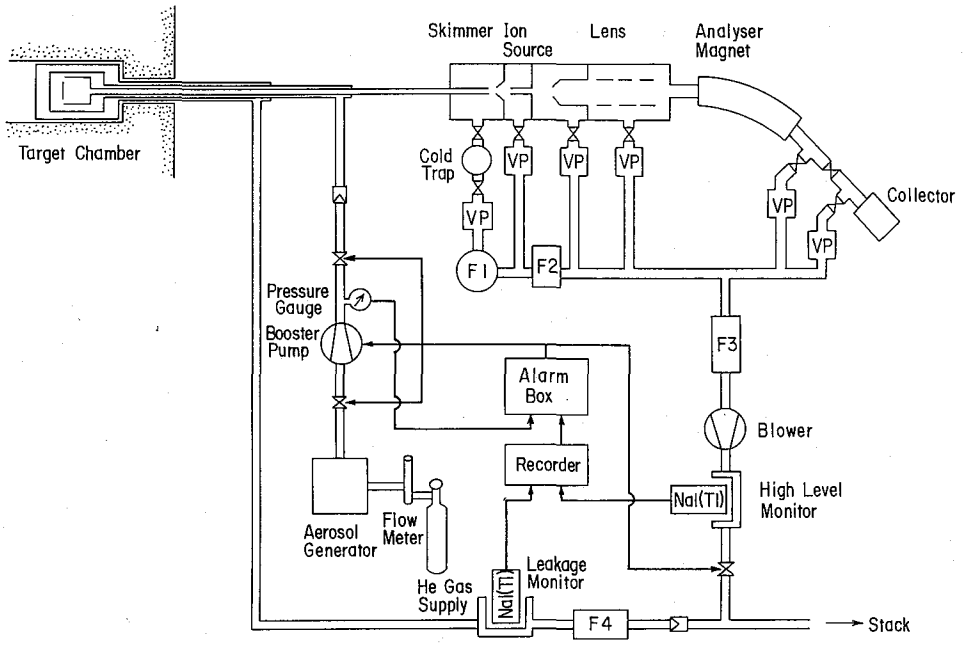

Fig. 1. Schematic diagram of the He-jet type KUR-ISOL. The helium flow path is explicitly shown. A small amount of oxygen is added to helium in the case of oxidation method. VP: vacuum pump; F 1~F 3: filters and cooling chambers.

to thermal velocity in a helium gas atmosphere (1~3 atm) and are attached to DOP (dioctylphthalate) aerosols. After transported through a capillary of 1.0 mm in inner diameter and a two-stage flat-skimmer chamber in a few seconds, the fission products are ionized by an ion source[2,3]. The ionized activities are extracted from the ion source and focused in a parallel beam by accelerating and focusing electrodes. The activities mass-separated by an analyzer magnet are collected on an Al-coated Mylar tape to perform the nuclear spectroscopic studies on neutron-rich nuclei as will be described below. The available intensity of the individual isotope depends on the independent or cumulative fission yield, the half-life and the ionization efficiency of the relevant isotope. Main specifications of the KUR-ISOL facility are listed in Table 1.

ii) *Aerosol material*

As aerosol materials for the transportation of fission products, we have tested diffusion pump oil, DOP and alcohol in the test stage of ISOL[4]. DOP is well known as a standard material for aerosol generation, and has been adopted since then because it showed rather high and stable transport efficiency using NaCl as seed material. In recent years, however, it was claimed that the low melting-point material is liable to evaporate in front of a high-temperature ion source and rather high melting-point materials such as KCl, $PbCl_2$, $MgCl_2$, $ZnBr_2$ or PbI_2 are suitable for ISOL. In particular, $PbCl_2$ was reported to give the highest transport efficiency[5]. The overall efficiency of our system in cases of high melting-point aerosol materials ($PbCl_2$ and CsCl) for a He-jet has therefore been tested, measuring the ^{94}Rb beam intensity as a function

Table 1. Main specifications of KUR-ISOL.

He-jet ; DOP+NaCl (seed) aerosol type with O_2 admixture for oxidation method

He pressure	1～2 atm	max 3 atm
He flow rate	1000～1500 atm・cc/min ; stabilized by thermo-resistive flow meter feedback	
O_2 flow rate	0.5～5.0 atm・cc/min	
Capillary	1.0 mm inner dia. ×11 m	

Ion source ; High-temperature thermal type

Filament voltage	6～8 V	max	12 V
Filament current	50～70 A	max	100 A
Bombarding voltage	400 V	max	750 V
Bombarding current	0.2～1 A	max	2 A ; stabilized by filament feedback
Temperatue		max	3000 °C

Accelerating and focusing system ; Electrostatic lens focusing to parallel beam

Extraction voltage	14 KV	max	30 KV ; stability $<\pm 0.5\%$
Acceleration voltage	30 KV	max	40 KV ; stability $<\pm 0.005\%$
Focusing voltage	～14 KV	max	30 KV ; stability $<\pm 0.005\%$

Mass analyzing system ; Sector-type uniform field with fringing field vertical focusing

Deflection radius	600 mm
Pole gap	40 mm
Deflection angle	45°
Entrance (ε_1) and exit (ε_2) angles	$\varepsilon_1=26.2°$; $\varepsilon_2=0°$
Magnetic field	max 0.8 T ; stability $<\pm 0.005\%$
Mass resolution	600

Vacuum system

He-jet 1st stage	1200 m³h	Roots pump+930ℓ /min rotary pump
He-jet 2nd stage	600 m³/h	Roots pump+450ℓ /min rotary pump
Extraction chamber	6″ 820ℓ /s	diffusion pump+765ℓ /min rotary pump
Lens chamber	6″ 1500ℓ /s	diffusion pump+450ℓ /min rotary pump
Analyzing chamber	3″ 220ℓ /s	diffusion pump+200ℓ /min rotary pump
Collector chamber	4″ 310ℓ /s	turbo-molecular pump+200ℓ /min rotary pump

Active gas cooling and filter system

1st stage	60ℓ cooling chamber with two-stage glass wool filters
2nd stage	200ℓ cooling chamber with two-stage glass wool filters
3rd stage	250ℓ ×4 cooling chambers with two-stage glass wool filters*
4th stage	15ℓ chamber with charcoal, absolute and silver zeolite filters

Tape collector

Tape width	12.5 mm
Tape speed	max 1000 mm/s
Tape length	1000 m
Tape drive cycle	min 0.1 s

Ion yield

^{94}Rb	5×10^5 atm/s
^{152}Nd	5×10^4 atm/s

*Now under construction.

Table 2. Relative ion (^{84}Rb) yield for three kinds of cluster materials tested.

Material	Optimum temperature (°C)	Relative ion yield
DOP*	110	100
$PbCl_2$	400	50
CsCl	530	65

*NaCl is added as seed for aerosol generation.

of temperature of the heating oven of these materials. The results are shown in Table 2. No improvement of overall efficiency was found by the use of materials other than DOP. The calculation also indicated that the heating up of aerosol droplets by the radiation from the high-temperature ion source during their passage between the flat-skimmer chamber and the ion-source entrance is inadequate for their evaporation.

iii) *Skimmer system*

As a skimmer system to pump-off helium gas used for the transportation of aerosol material, a two-stage skimmer system has been adopted in the KUR-ISOL as the calculation indicated that the single-stage system was not enough to keep good vacuum conditions inside the separator itself. Recently, Dr. T. Karlewski, a visiting scientist from Mainz University, tried a single-stage system coupled with the Mainz-type thermal ion source, as schematically shown in Fig. 2. To test this system, a Roots pump with a pumping speed of 600 m^3/h was replaced to a larger one of 1200 m^3/h capacity. As the merit of this system is the increase of the acceptance angle of the ion source to a He-jet, the two-stage system with improved geometry was also tested, using the 600 m^3/h Roots pump as a second-stage pump. The three kinds of

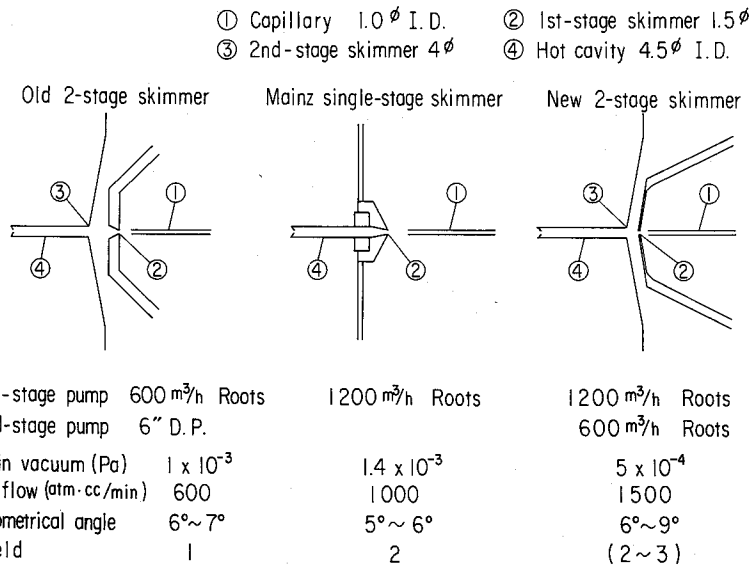

Fig. 2. Three geometries of thermal ion source and skimmer combinations tested.

geometry so far tried and the performances of these are compared in Fig. 2. The vacuum conditions of the separator were worse for the single-stage as expected, although the loss in mass resolution remained in 10%. The gain in the yields for the single-stage system was not so large as expected, but this may be improved in future.

iv) *High-temperature thermal ion source*

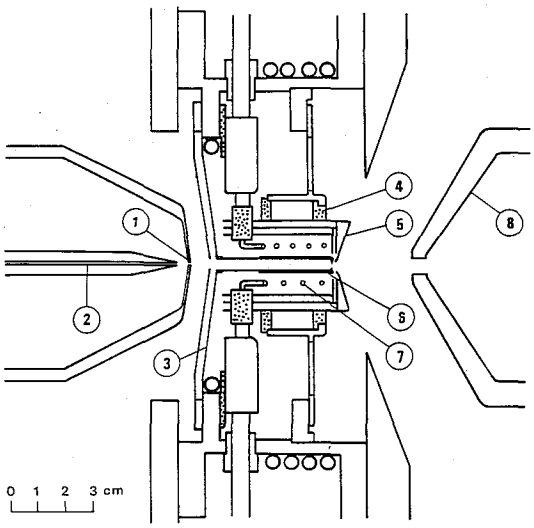

Fig. 3. Cross sectional view of a high-temperature thermal ion source for the He-jet type KUR-ISOL. ① Skimmer, ② capillary, ③ conical base plate (Mo), ④ insulator (BN), ⑤ thermal shields (Ta and Mo), ⑥ ionization chamber (W), ⑦ filament (W), ⑧ extractor (C).

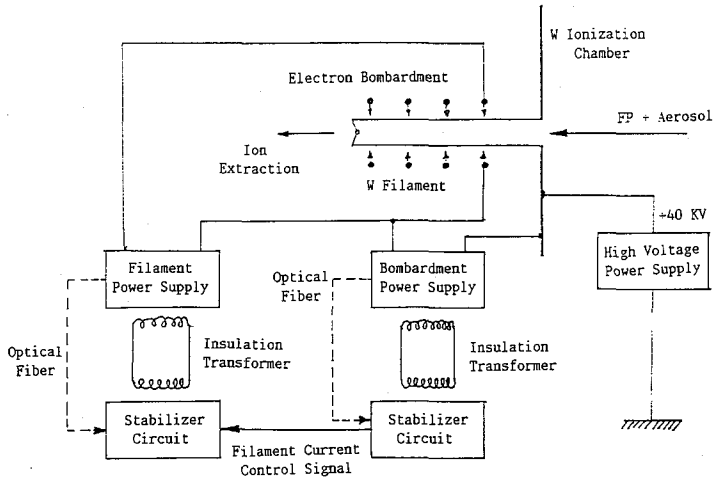

Fig. 4. Block diagram of a stabilizer system for electron-bombardment current utilizing feedback to the filament power supply. The bombarding voltage and current are manually set to some appropriate values, which are kept constant within ±0.5%. The error signal detected is fed back to a stabilizer circuit at ground potential by optical fibers to control filament power.

It is the most characteristic merit of the He-jet fed ISOL that the time delay of the activity-transportation process due to the adsorption at the surface or to the diffusion in the target matrix does not occur even for high melting-point elements. In order to obtain high ionization efficiency for rare-earth elements, a high-temperature thermal ion source has been constructed. Its cross sectional view is shown in Fig. 3. The ionization chamber consists of a tungsten cylinder 5.0 mm in inner diameter and 52 mm in length. The cylinder has an outlet hole of 0.8 mm in diameter at the front end. The front half of the cylinder is heated by the radiation from a tungsten filament of 1.5 mm in diameter situated outside the cylinder as well as by the bombardment of electrons. The cylinder and the filament are covered by a four- or five-fold thermal shield made of tantalum and molybdenum. The potential of the filament and the shield is kept at about -400 V with respect to the cylinder, with the bombardment current variable up to more than 1.0 A.

In an electron-bombardment type ion source, the instability of bombarding current and temperature is liable to occur because of the positive feedback action between temperature and bombarding current from filament. In order to stabilize the bombarding current and temperature, a stabilizer system as shown in Fig. 4 has been designed and incorporated into the power supply of the ion source. The filament voltage is controlled to maintain the bombarding current to a desired value. Without this system, it is almost impossible to keep the ISOL beam intensity constant for a period long enough for experimental works.

v) *Oxidation method*

Another way to obtain ions of rare-earth elements at high efficiency is the

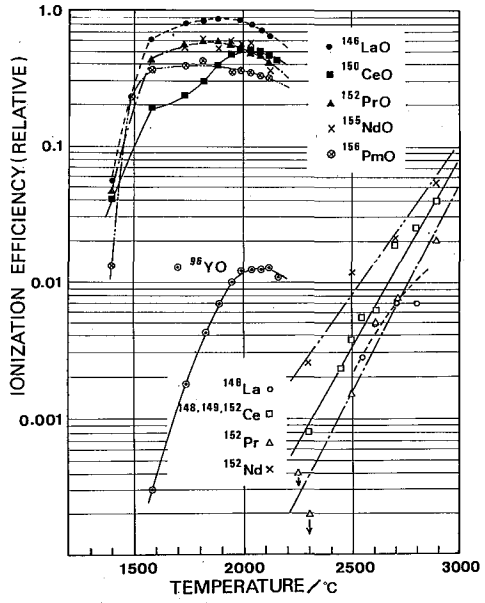

Fig. 5. Ionization characteristics of light lanthanide monoxides as a function of ionizer temperature[6].

oxidation technique by which metallic atoms are converted to monoxide compounds and the ionizer surface is covered with an oxygen-rich layer. It is known that monoxides of light lanthanides (LaO, CeO, PrO, NdO and PmO) have low ionization potentials (about 4.9 eV) and the work function of a tungsten surface with oxygen adsorption is enhanced up to 6.2 eV. These are superior conditions for the efficient surface ionization.

By introducing a small amount of oxygen gas into a He-jet, very high ionization efficiencies could be achieved with the high-temperature thermal ion source described above[6]. In Fig. 5, ionization characteristics for light lanthanides are demonstrated as a function of the ionizer temperature. The ionization efficiencies are enhanced several ten times or more as compared with the case of metallic ions and maximum yields are obtained at relatively low temperature (about 2000°C), which is very convenient for stable operation of the ion source.

vi) ***Tape collector***

The mass separated radioisotopes are collected on an Al-coated Mylar tape. The tape driving system should satisfy requirements to move a tape as fast as possible and to stop it at the measuring position as accurately as possible. Moreover, the high vacuum should be kept inside the collector from view points of ion beam optics and the conversion electron spectroscopy.

The specifications of the present tape system are described in Table 1. It can drive a 12.5 mm wide tape at a maximum speed of 1000 mm/s. External controls are possible in connection with a control device. The vacuum problem is solved by adopting magnetic fluid seal units.

vii) ***Measuring system***

In order to identify a new isotope, it is important to measure half-lives of X-rays and γ-rays accurately for the discrimination of shorter-lived components against the huge number of longer-lived contaminating background radiations. For this purpose, a low-energy photon spectrometer (LEPS) with the area of 500 mm^2 and a 132 cm^3 n-type coaxial HPGe X-γ detector have been used. The latter has the efficiency of 32.5% relative to that of 3″x 3″ NaI at 1.33 MeV. The full-width at half-maximum energy resolutions were 740 eV and 1.84 keV at 6.4 keV and 1.33 MeV, respectively. The detector and a tape-collector chamber were completely shielded by lead blocks 10 cm thick and boron-carbide plates to reduce room backgrounds near the reactor KUR. The inner surfaces of the lead blocks were covered with copper plates 9 mm thick and aluminum plates 1 mm thick to suppress Pb and Cu X-rays. The energy calibration was performed by using sources of ^{241}Am, ^{152}Eu, ^{137}Cs and ^{60}Co before and after the measurements. The efficiency curve between 30 keV and 3.5 MeV was constructed using a set of calibrated sources.

The measurements were continuously repeated during several days with a moving tape collector and a time-resolved spectroscopy systm. The latter was especially designed for our experiments almost 10 years ago and was manufactured by the Laboratory Equipment Corporation Co. using an 8 bit MBC-225 microcomputer then

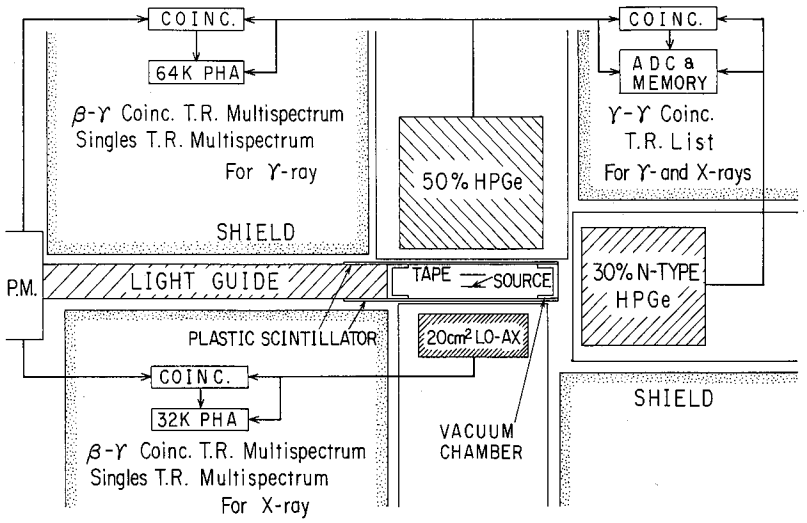

Fig. 6. Geometrical configuration of a $4\pi\beta$-γ, $4\pi\beta$-X and γ-γ coincidence measuring system using two 80 mm×80 mm×1 mm plastic scintillators, 50% and 30% HPGe γ-ray detectors and a HPGe low-energy photon detector.

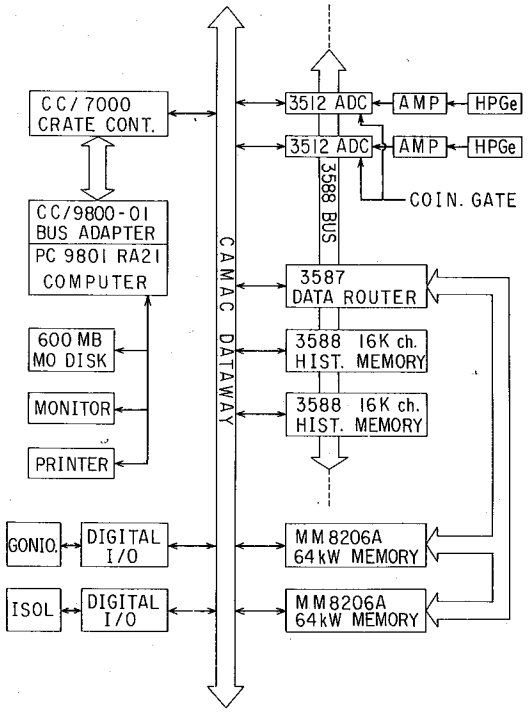

Fig. 7. Block diagram of a CAMAC data acquisition system for time-resolved multi-spectrum and time-resolved list-mode measurements.

available. It allowed sequential spectrum scaling up to 4 k-channels×16, 2 k-channels×32 or 1 k-channels×64, started by the signal from the controller of ISOL and the tape collector. The computer of this system was afterwards replaced to a faster machine (16 bit PC-9801 VX) with DMA data transfer capability.

For the studies of nuclei far from stability, it is generally important to install high-efficiency detecting systems and to measure several physical quantities simultaneously as the source intensity and the machine time are rather limited. Especially for the identification of a new isotope, X-ray and β-γ coincidence measurements are usually essential for Z determination and for the discrimination against the possibility of an unknown isomer. The γ-ray singles and γ-γ coincidence measurements with high efficiency are also important, of course. In order to perform these experiments simultaneously and efficiently, a $4\pi\beta$-γ coincidence system has been constructed. Its arrangement is conceptually shown in Fig. 6.

As can be seen from Fig. 6, several sets of a time-resolved spectroscopy system and a time-resolved list-mode coincidence data storage system are necessary. For this purpose, a CAMAC data acquisition system consisting mainly of LeCroy nuclear spectroscopy modules has been prepared. The CAMAC system as shown in Fig. 7 allows not only time-resolved spectroscopy up to 256 k-channels (4 k-channels×32), but also time-resolved multi-dimensional list-mode data storage to a 600 MB magneto-optical (MO) disk. The data transfer time to the MO disk is now about 30 kB/s using our assembler-linked FORTRAN program. Another advantage of this system is the capability to control ISOL and other experimetal apparatus through the CAMAC dataway.

EXPERIMENTAL PROCEDURES AND RESULTS

As the methods of identification are somewhat different for each isotope, the experimental procedures and results for four isotopes are described in historical order.

i) ^{156}Pm

As the vapor pressure of promethium is rather high at the temperature of ion source, it could be ionized in moderate intensity without the use of oxidation method. At mass 156, several new γ-ray lines with short half-lives have been observed. In particular, three lines with energies 75.8±0.6 (37±10), 174.2±0.1 (100) and 267.4±0.5 (19.7±1.4) keV (relative intensities of γ-rays normalized to the 174.2 keV line are shown in the brackets) were found to decay with the half-life of 35±13, 30.3±2.4 and 26.9±6.0 s, respectively. These energies agree well with the values expected from the level scheme of ^{156}Sm[7,8] as the transitions between ground state rotational band. The K_α and K_β X-rays of Sm observed also showed hafl-lives of 28.1±1.8 and 32.0±3.9 s, respectively. Then the new isotope ^{156}Pm was concluded to decay with the half-life of 29±2 s[9].

With increased beam intensity of Pm by the oxidation method, more precise measurements have recently been performed and 26 new γ-rays were observed[10] in addition to the 9 lines reported using an ISOL with a ^{252}Cf source[11]. The half-life was

newly determined as 27.0 ± 0.3 s[10].

ii) ^{155}Nd

The search for X-rays and γ-rays originating from the unknown isotope ^{155}Nd was performed at the mass 155. As the ionization efficiency for promethium is rather high compared to that for neodymium, radiations originating from the 48 s ^{155}Pm activity were considerable and no trace of Pm X-rays was observed in the original spectra. By

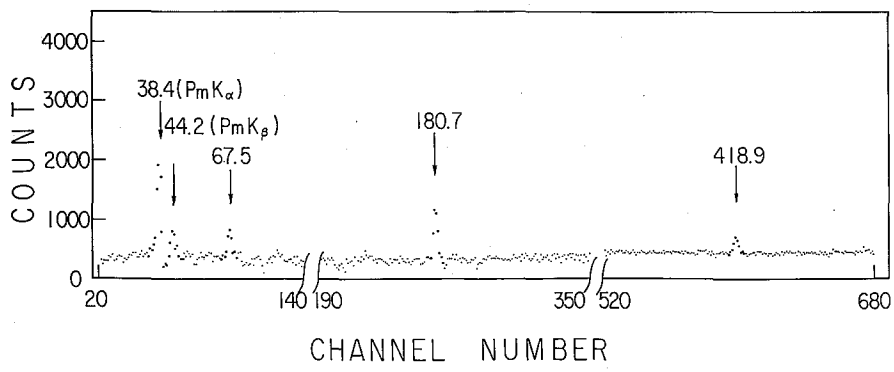

Fig. 8. Gamma-ray singles spectrum obtained at mass 155 by subtracting the contributions of ^{155}Pm activity and of longer-lived activities.

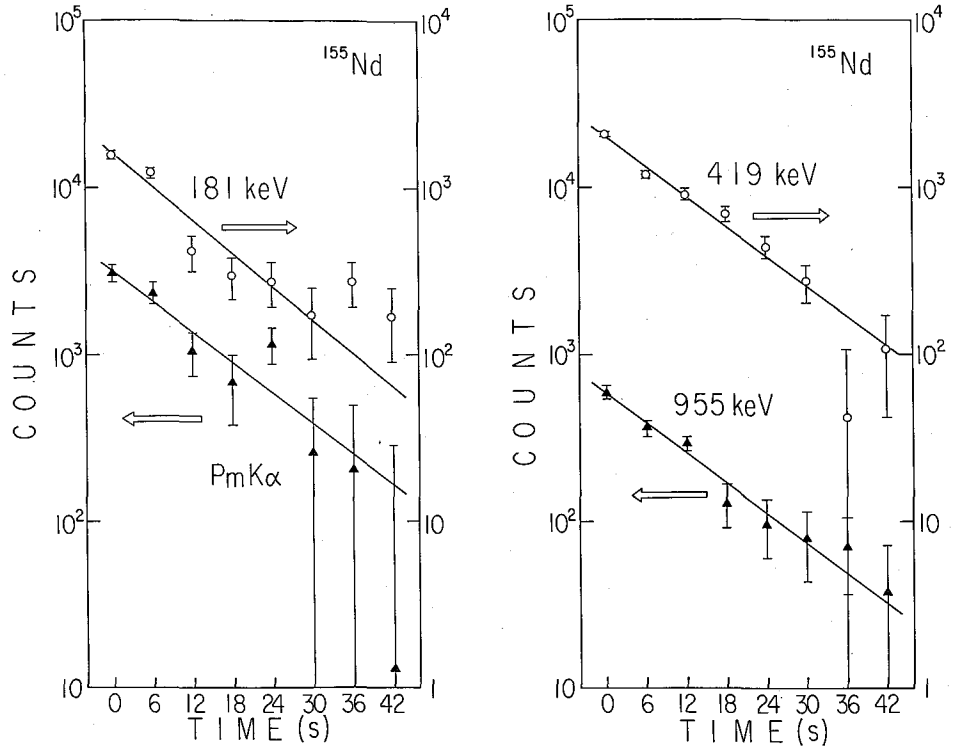

Fig. 9. Decay curves of Pm K_α X-ray and three γ-ray lines assigned to the decay of ^{155}Nd.

subtracting the successive sixteen spectra using a multiplying factor to cancel the contributions of the 48 s ^{155}Pm activity, a spectrum as shown in Fig. 8 was obtained. Four lines with energies 67.5±0.3 (29±5), 180.7±0.2 (100±6), 418.9±0.3 (82±12) and 955.1±0.3 (48±16)(relative intensities of γ-rays normalized to the 180.7 keV line are shown in the brackets) were observed with the half-life of 11.5±4.5, 9.2±0.9, 9.6±1.3 and 10.0±1.5 s, respectively. In addition, Pm K_α X-ray was found to decay with the half-life of 10.0±2.0 s. The decay curves obtained are shown in Fig. 9.

In order to reject the possibility that these radiations might originate from the unknown isomer of ^{155}Pm, the yields of the four γ-rays mentioned were measured as a function of ion-source temperature. The temperature dependence of the yields of these γ-rays observed was similar to that of the well known 151.9 and 850.5 keV lines following the decay of ^{154}Nd, but was markedly different from that of 725.4 and 778.6 keV lines and Sm X-rays which follow the decay of ^{155}Pm. This showed that the ion-source chemistry is a powerful tool to identify which element emits newly found radiations.

The half-life of ^{155}Nd has been determined as 9.5±0.7 s averaging the several observed values[12]. Another value of 8.9±0.2 s has been reported later[11].

iii) ^{154}Pr

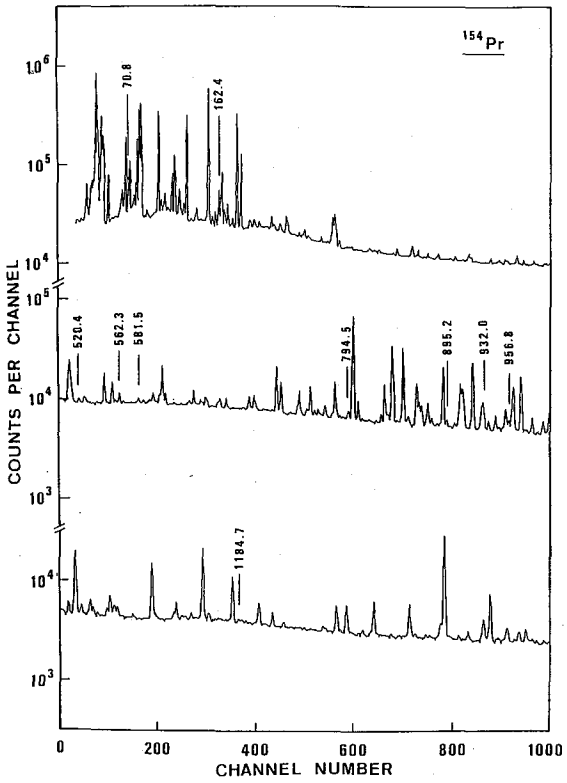

Fig. 10. Gamma-ray singles spectrum of ^{154}Pr taken with an HPGe detector.

The heaviest isotope of praseodymium, ^{154}Pr, was identified for the first time by γ-ray measurements of mass separated activities. The $A=154$ activities were obtained by adding oxygen gas at a flow rate of 0.5 ml/min. The optimum conditions of the whole system were determined by utilizing the 25.9 s ^{154}Nd activity. Gamma-ray multi-spectra measurements were carried out with a high-resolution HPGe detector for low-energy γ-rays and X-rays and with a 30% HPGe detector for high-energy γ-rays. The spectrum obtained is shown in Fig. 10. From the half-life measurements on the observed γ-lines, 10 γ-rays and the Nd X-rays were found to decay at a half-life of 2.3 (1) s. It is then concluded that these short-lived components are generated by the β-decay of ^{154}Pr[13]. The observed 70.8 and 162.4 keV γ-rays correspond to the 2^+-0^+ and 4^+-2^+ transitions in ^{154}Nd, respectively. The spin and parity of the ground state of ^{154}Pr is considered to be 3^+ because the log ft values to the 4^+ and 2^+ levels in ^{154}Nd are estimated to be about 5.4 and 4.8, respectively, and no β-feeding was found to the 6^+ level in ^{154}Nd.

iv) ^{152}*Ce*

Although the ^{152}Ce isotope was once reported as identified to decay with the half-life of 3.1 (3) s[14], the γ-γ coincidence experiments on ^{152}Pr showed that the 285 keV γ-ray, a single γ-ray line assigned to the ^{152}Ce decay, belongs to the decay of ^{152}Pr[15]. The search for ^{152}Ce has been carried out by means of γ-ray and X-ray decay measurements. The experimental procedure is almost the same as the ^{154}Pr case except that the optimum values of the collection and measuring times for ^{152}Ce were chosen. Two γ-ray lines at 97.8 and 114.8 keV were found to have shorter half-lives than ^{152}Pr. The Pr X-K_α line was observed to decay with the same half-life. In order to ascertain that these short-lived components are generated certainly by the β-decay of ^{152}Ce, the β-γ coincidence was measured with a 1 mm thick Al absorber to suppress the contribution of internal conversion electrons. The 97.8 keV transition was confirmed to be in full coincidence with the β-ray. The 114.8 keV transition, however, was found to be delayed about 1 μs.

It is then concluded that the two γ-rays and the Pr-K_α X-ray are generated by the β-decay of ^{152}Ce with a half-life of 1.4 (2) s[16].

DISCUSSIONS

i) *Half-life of NFFS*

The half-lives of unknown nuclides lying far from the stability line have first been predicted by Takahashi, Yamada and Kondoh using a gross theory of β-decay[17]. This theory has been modified recently and revised values of predicted half-lives have been published by Tachibana *et al*[18,19]. The predicted values depend on the width of the GT single-particle strength distribution (case 1 and case 2) and also on the parameter ΔQ_0 (case a, case b and case c) which is a measure of the excitation-energy range to which the transitions are highly forbidden. The predicted values of this theory for four isotopes identified here are listed in Table 3.

After about 10 years since the pioneering work of Takahashi *et al.*, Klapdor,

Table 3. Comparison between theoretically predicted half-lives and experimentally obtained values.

Nuclide	Theoretically predicted half-life (s)								Experimental half-life (s)	
	Gross theory[a]						Microscopic theory			
	Case								Present	Others
	1a	1b	1c	2a	2b	2c	TDA[b]	pn-QPRA		
^{152}Ce		2.13			3.39		1.97	2.19[c]	1.4(2)[d]	
^{154}Pr	2.53	2.83	4.96	3.97	4.43	7.72	1.46	2.72[e]	2.3(1)[h]	
								2.14[f]		
								0.882[g]		
^{155}Nd	7.26	11.1	17.2	11.4	17.3	26.8	15.3	14.84[c]	9.5(7)[i]	8.9(2)[j]
^{156}Pm	19.3	27.0	111	29.6	41.3	170	8.39	38.93[k]	27.0(3)[l]	28.2(11)[m]
										26.70(10)[n]

[a]Ref. (19). [b]Ref. (20). [c]A. Staudt, private communication; Q_B-value from ref. (21) is used. [d]Ref. (16). [e]Ref. (28); mass formula of ref. (22) is used. [f]Ref. (28); mass formula of ref. (23) is used. [g]Ref. (28); mass formula of ref. (24) is used. [h]Ref. (13). [i]Ref. (12). [j]Ref. (11). [k]A. Staudt, private communication; Q_B-value from ref. (25) is used. [l]Ref. (10). [m]Ref. (26). [n]Ref. (11).

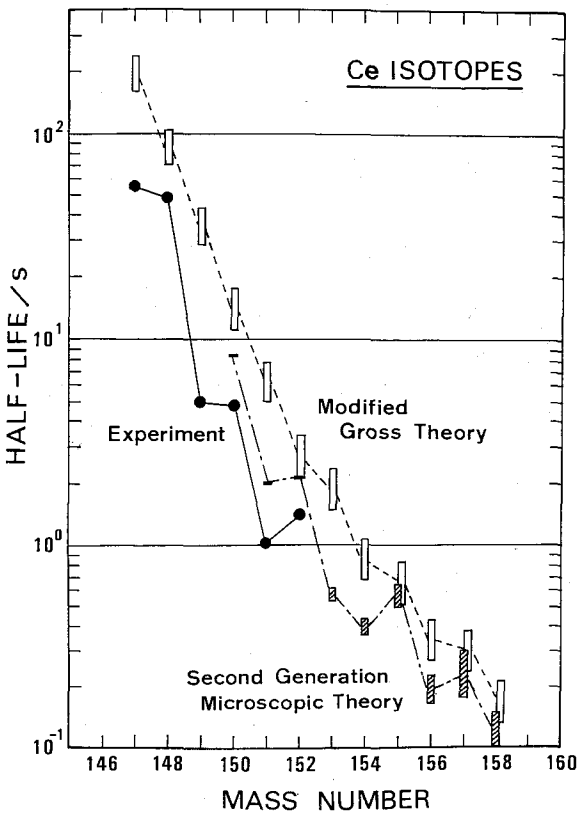

Fig. 11. Half-lives of Ce isotopes. The upper and lower limits of the bar shown for the modified gross theory[18,19] correspond to the predicted values in the cases of 2b and 1b, respectively, of ref. (19). In the case of the second generation microscopic theory[27,28], upper and lower limits shown for mass number between 153 and 158 correspond to the predicted values by using the mass formulae of ref. (23) and ref. (22), respectively. For mass number 150, 151, and 152, the predicted values shown are from A. Staudt (private communication) calculated with Q_β-values of refs. (25), (25), and (21), respectively.

Metzinger and Oda have published beta-decay half-lives of neutron-rich nuclei calculated by a microscopic theory using Tamm-Dancoff approximation (TDA)[20]. This prediction was considered to improve the gross theory particularly in regions far from stability. This microscopic approach has recently been revised to a second generation version using the proton-neutron quasiparticle random phase approximation (pn-QRPA) with a schematic GT residual interaction[27]. The predicted values of these calculations[28] are also listed in Table 3 together with the experimental values.

A comparison of our experimental results with these predictions shows that the predicted values of the gross theory in case of 1a or 1b agree rather well with experimental values. As to the microscopic theory, the predicted half-lives for ^{154}Pr and ^{156}Pm have been much improved in the new version. No marked alterations of predicted values are seen in the cases of other nuclides listed in Table 3.

In Fig. 11, experimental half-lives of Ce isotopes are compared with theoretical predictions. It can be seen that the theoretical predictions are always larger than experimental values for Ce isotopes, although the rate of decrease with mass number is well reproduced. It can also be noticed that the even-odd effect clearly observed experimentally is not well reproduced in the case of gross theory. Both theories predict that the half-life decreases mainly at even mass number for $A \geqq 152$, but this is in contradiction with the general tendency experimentally observed that the half-life decreases mainly at odd mass number for even Z nuclei. Whether the predicted tendency really exists or not at these neutron-rich Ce isotopes is of interest.

ii) ***Moment of inertia and deformation***

Neutron-rich isotopes with mass number $150 \leqq A \leqq 190$ belong to the well-established deformed region of rare-earth nuclei. These nuclei show characteristic ground-state rotational band with the excitation energies

$$E_I = \frac{\hbar^2}{2\mathcal{I}} I\,(I+1)$$

for rotational states with angular momentum I. The moment of inertia $\mathcal{I}$ at the ground state can be derived from the excitation energy of the first excited state, E_{2+}, as $\frac{3\hbar^2}{E_{2+}}$ The moments of inertia of nuclei for rotational motion thus derived for even-even nuclei in this mass region are plotted in Fig. 12, together with the rigid-body values. The nuclei with the ratio of excitation energies E_{4+}/E_{2+} less than 3.0 have been omitted from plotting as these may not be well-deformed nuclei. It can be seen that the newly found moment of inertia for ^{154}Nd shows the largest value among those of known even-even nuclei in this mass region.

As can be seen from Fig. 12, the maximum moment of inertia for each isotope seems to decrease with mass number in this mass region, in contrast to the general tendency hitherto reported[31,32]. This may indicate that the deformation increases towards the neutron-rich light rare-earth nuclei. The fact that the moments of inertia observed are appreciably smaller than rigid-body values has been attributed to the pairing correlations in the intrinsic nucleonic motion. For quantitative explanation of the tendency as described, precise estimates of deformation parameters and pairing-

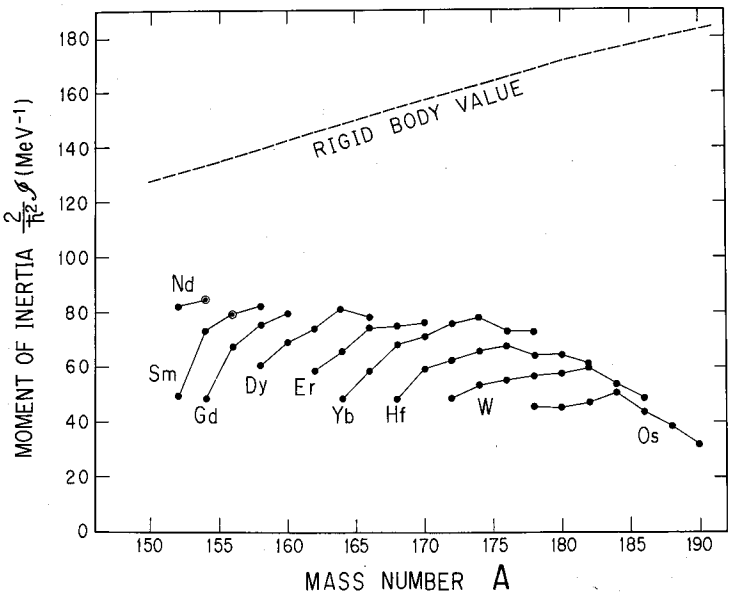

Fig. 12. Systematics of moments of inertia for even-even nuclei in the mass region $150 \leqq A \leqq 190$. The mark ◎ indicates that the moments of inertia have been derived from the present measurements. Other values have been derived from the energy levels cited in refs. (29) and (30).

energy gap parameters are necessary. Some calculations towards this direction are now in progress.

CONCLUDING REMARKS

The fission yields of isotopes far from the stability line decrease rapidly with neutron number as shown in Fig. 13. The newly identified isotopes here reported have cumulative fission yields of about 10^{-2}%. Still unknown isotopes such as ^{153}Ce, ^{155}Pr, ^{157}Nd or ^{159}Pm lie around 10^{-3}% in fission yields. To identify these isotopes, we are now preparing to increase the amount of ^{235}U target about 3 to 10 times. This necessitates the installation of large cooling and filter chambers to suppress the effects of active rare gases. The target chamber has to be cooled by the circulation of CO_2 gas if its temperature exceeds about 150 °C. Some preparatory works for this direction are now in progress.

The high efficiency $4\pi\beta$-γ detecting system described is not only a powerful tool for the identification of new isotopes, but also allows to establish precise decay schemes for very neutron-rich short-lived isotopes produced by fission as the decay schemes of a lot of nuclides lying near the edge of fission yields are still almost unknown. We have also prepared a β-γ coincident Si (Li) conversion electron spectrometer, a γ-γ angular correlation apparatus with four 30% HPGe detectors and a life-time measurement system with two BaF_2 detectors. With the help of these powerful tools for nuclear spectroscopic works on short-lived nuclei, the nuclear structure of a lot of neutron-rich nuclides in medium mass region can be studied

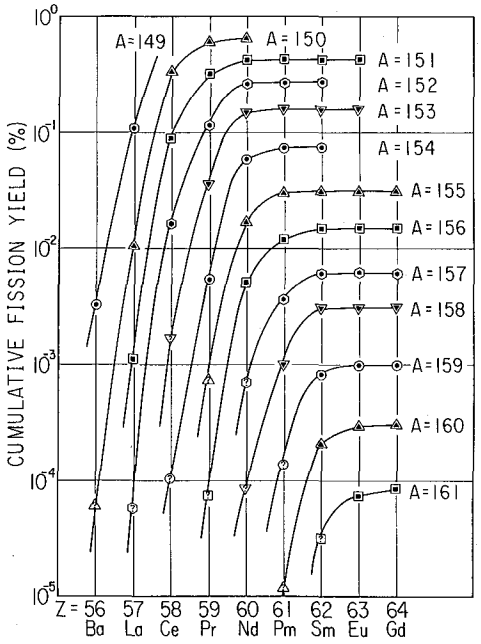

Fig. 13. Cumulative fission yields of rare-earth elements for thermal nuetron fission of ^{235}U. The mark? indicates that the corresponding nuclide is still unknown.

systematically through the decays of mass-separated isotopes produced by fission.

ACKNOWLEDGMENT

One of the authors (K. O.) would like to express his sincere thanks to Emeritus Professors H. Takekoshi and K. Kimura for their efforts and guidances in constructing and testing the isotope separator of the Institute for Chemical Research. The authors would like to express their sincere thanks to Drs. K. Aoki, S. Yamada, Y. Funakoshi, K. Kawade, I. Tago, T. Seo and other members of KUR-ISOL group for their co-operative works. Thanks are also due to a lot of members of our institute for the operation, maintenance and manufacturing of our experimental apparatus.

REFERENCES

(1) K. Kimura, J. Muto, I. Kumabe, H. Takekoshi, K. Okano, T. Tsuchimoto, M. Soneda, and Y. Kondoh, *Shitsuryou-bunseki (in Japanese)*, 8, 12 (1957).
(2) K. Okano, Y. Kawase, K. Kawade, H. Yamamoto, M. Hanada, T. Katoh, and I. Fujiwara, *Nucl. Instrum. Methods*, **186**, 115 (1981).
(3) Y. Kawase, K. Okano, and K. Aoki, *Nucl. Instrum. Methods in Phys. Res.*, **B 26**, 341 (1987).
(4) K. Kawade, H. Yamamoto, K. Okano, Y. Kawase, and I. Fujiwara, *Kyoto Univ. Res. Reactor Inst. Technical Report* KURRI-TR-**146**, 23 (1976).
(5) M. Brügger, N. Hildebrand, T. Karlewski, N. Trautmann, A. K. Mazumdar, and G. Herrmann, *Nucl. Instrum. Methods in Phys. Res.*, **A 234**, 218 (1985).

(6) Y. Kawase, and K. Okano, *Nucl. Instrum. Methods in Phys. Res.* **B 37/38**, 116 (1989).
(7) W. John, F. W. Guy, and J. J. Wescolowski, *Phys. Rev.* **C 2**, 1451 (1970).
(8) J. B. Wilhelmy, S. G. Thompson, R. C. Jared, and E. Cheifetz, *Phys. Rev. Lett.*, **25**, 1122 (1970).
(9) K. Okano, Y. Kawase, and Y. Funakoshi, *J. Phys. Soc. Jpn.*, **55**, 715 (1986).
(10) K. Okano, and Y. Kawase, *Annu. Rep. Res. Reactor Inst. Kyoto Univ.* **22**, 92 (1989).
(11) R. C. Greenwood, R. A. Anderl, and J. D. Cole, *Phys. Rev.* **C 35**, 1965 (1987).
(12) K. Okano, and Y. Kawase, *Radiochimica Acta,* **40**, 57 (1986).
(13) Y. Kawase, and K. Okano, *Z. Phys. A-Atomic Nuclei,* **330**, 231 (1988).
(14) J. C. Hill, H. Yamamoto, and A. Wolf, *Phys. Rev.* **C 27**, 2857 (1983).
(15) T. Karlewski, N. Hildebrand, M. Brügger, N. Kaffrel, N. Trautmann, and G. Herrman, *Z. Phys. A-Atomic Nuclei,* **330**, 55 (1988).
(16) I. Tago, Y. Kawase, and K. Okano, *Z. Phys. A-Atomic Nuclei,* **335**, 477 (1990).
(17) K. Takahashi, M. Yamada, and T. Kondoh, *At. Data Nucl. Data Tables,* **12**, 101 (1973).
(18) T. Kondoh, T. Tachibana, and M. Yamada, *Prog. Theor. Phys.*, **74**, 708 (1985).
(19) T. Tachibana, M. Yamada, and K. Nakata, *Report of Sci. and Eng. Res. Lab. Waseda Univ.* No. **88-4** (1988).
(20) H. V. Klapdor, J. Metzinger, and T. Oda, *At. Data Nucl. Data Tables,* **31**, 81 (1984).
(21) A. H. Wapstra, G. Audi, and R. Hoekstra, *At. Data Nucl. Data Tables,* **39**, 281 (1988).
(22) E. R. Hilf, H. v. Groote, and K. Takahashi, *CERN Report* **76−13**, 142 (1976).
(23) H. v. Groote, E. R. Hilf, and K. Takahashi, *At. Data Nucl. Data Tables,* **17**, 418 (1976).
(24) P. Möller and J. R. Nix, *At. Data Nucl. Data Tables,* **26**, 165 (1981).
(25) A. H. Wapstra, and G. Audi, *Nucl. Phys.* **A 432**, 1 (1985).
(26) H. Mach, A. Piotrowski, R. L. Gill, R. F. Casten, and D. D. Warner, *Phys. Rev. Lett.*, **56**, 1547 (1986).
(27) A. Staudt, E. Bender, K. Muto, and H. V. Klapdor, *Z. Phys. A-Atomic Nuclei,* **334**, 47 (1989).
(28) A. Staudt, E. Bender, K. Muto, and H. V. Klapdor, *At. Data Nucl. Data Tables,* **44**, 79 (1990).
(29) Table of Isotopes, 7 th edition, ed. C. M. Lederer, and V. S. Shirley (1978).
(30) M. Sakai, *At. Data Nucl. Data Tables,* **31**, 399 (1984).
(31) S. G. Nilsson, and O. Prior, *Mat. Fys. Medd. Dan. Vid. Selsk.,* **32**, no. 16 (1960).
(32) A. Bohr and B. R. Mottelson, Nuclear Structure, vol II, p. 74, Benjamin, Massachusetts, 1975.